

Finite Element Analysis of Pushout Test for Stirrup Shear Connector

Hussein R. Lazim^{1,*}, Nabeel Abdulrazzaq Jasim²

^{1,2} Department of Civil Engineering, College of Engineering, University of Basrah, Basrah, Iraq

E-mail addresses: hussein_raheem80@yahoo.com, nabeel_ali58@yahoo.com

Received: 12 November 2022; Revised: 20 December 2022; Accepted: 8 January 2023; Published: 2 July 2023

Abstract

This numerical study was conducted to simulate and analyze the pushout test for the new shear connector in a new steel-concrete composite system. In this system, the shear stirrups of the reinforced concrete beam are used as shear connectors when passed through holes drilled in the web of inverted steel T-section. The numerical analysis was performed by creating a three-dimensional finite element model using the finite element program ANSYS 21 student version to simulate the behavior of the new innovative shear connectors. The pushout specimens analyzed in this study have been tested experimentally by the same researchers earlier. A total of fifty-six push-out specimens were modeled and analyzed to investigate the effect of many parameters on the shear strength and slip capacity of the shear connector. The parameters studied in this investigation were the specimen dimensions (length and width), the diameter of stirrups (shear connector), the number of connectors per specimen, concrete strength, size of T-section, and shape of the specimen. The finite element analysis using ANSYS gave a good prediction of the effect of studied parameters on connector strength, the failure modes, the form and intensity of deformations in the model, and the load-slip response. The maximum difference in connector strength which was observed between the numerical and experimental results was 15 %.

Keywords: Finite element, Pushout test, Stirrups, Shear connector, Composite reinforced concrete.

© 2023 The Authors. Published by the University of Basrah. Open-access article.

<https://doi.org/10.33971/bjes.23.1.5>

1. Introduction

Composite steel-concrete systems are commonly utilized in building and bridge construction. A composite system is formed when a concrete member, like a bridge or floor slab, is attached to supporting steel components, like I-section beams. In a composite member, the concrete's relatively high compression strength supplements steel's strong tensile strength. Due to the composite action of steel and concrete, composite steel-concrete structures have a high load-carrying capacity, relatively high stability, and high stiffness [1]. Composite action between the steel and reinforced concrete depends on the connection between these two elements. This connection is normally achieved by adding shear connectors at the contact region.

The shear connectors are the key element for successful composite action, which allow forces in the steel to be transferred to the concrete and vice versa, as well as resist uplift forces developed at the steel-concrete interface region.

In composite construction, a variety of shear connector types have been developed and utilized. The common type is shear connectors fixed on the flange of steel girders to provide the required shear transfer between the steel girders and slab. The headed stud, also known as a shear stud Fig. 1 (a), is the most common one in this type of shear connector. Perfobond, crestbond, angle, T-shape, and channel connectors, are other types of shear connectors, Fig. 1.

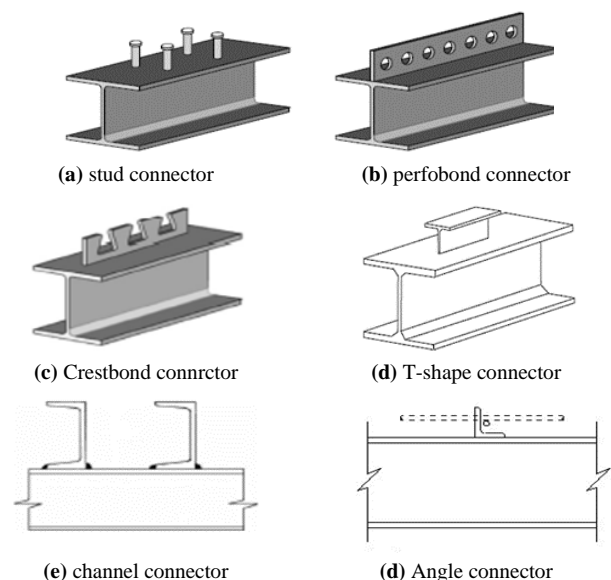


Fig. 1 Types of shear connectors.

1.1. Composite reinforced concrete

Another type of composite system called composite reinforced concrete CRC was suggested by Taylor [2]. In this type, normal composite construction, Fig. 2 (a), has been changed to something very close to reinforced concrete, Fig. 2 (c). In fact, this new system is reinforced concrete with external reinforcement. Composite reinforced concrete CRC

achieves the combination of the constructional advantages of composite construction with the material advantage of reinforced concrete.

The cross section of a CRC beam consists of a steel channel at the beam's soffit connected to reinforced concrete by shear connectors, Fig. 2 (b). The shear connectors may be shear studs welded to the web of channel section, transverse bolts, or transverse bars passing through holes drilled in the channel flanges [3].

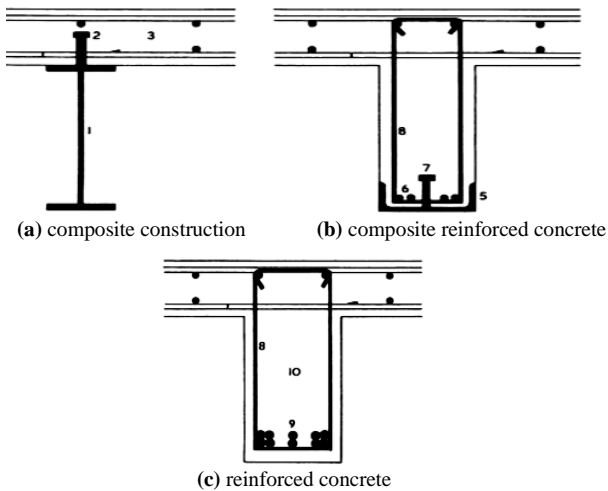


Fig. 2 Cross sections for three types of constructions [2].

A new type of CRC has recently been proposed by [4] Witwit and Abdulrazzaq [4]-[6]. The steel channel section was replaced with a steel T-section in the new structural material, and shear stirrups of reinforced concrete were used as shear connectors. In terms of supporting the form for casting the concrete floor, the steel T-section outperforms the channel section. Furthermore, because the new system does not require any additional shear connectors, the preparation for connecting the steel T-section to the reinforced concrete only requires drilling holes in the web of the steel T-section through which the stirrups will pass, Fig. 3.

This numerical study was conducted to simulate and analyze the pushout test for the new shear connector in a new steel-concrete composite system. The pushout specimens analyzed in this study have been tested experimentally by the same researchers earlier [7]. The main objectives of this paper are the (i) determination numerically of strength of the stirrup shear connector in the new CRC system using the ANSYS 21 program and (ii) the construction of the load-slip relationship of the connector. Comparing between the numerical and experimental results is also made.

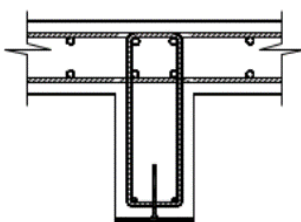


Fig. 3 New suggested section for CRC [4].

2. Push-out tests

The behavior of shear connections can be predicted by either experiments or finite element analysis. Experimentally,

to establish the load-slip characteristics and ultimate capacity of shear connectors, push-out tests can be used [8].

The push-out test is the most common method used to determine the shear strength and investigate the behavior of shear connectors. Many researchers have conducted extensive studies to investigate the behavior of most of the shear connectors under this type of test. Fig. 4 illustrates the details of the EN 1994-1-1 [9] standard push-out test. The two slabs are placed on the bottom plate of a frame or testing machine, and the load is directly applied to the steel I-section. In order to plot the slip vs. the load per connector, the slip between the steel I-section and the slabs is measured at various points [1].

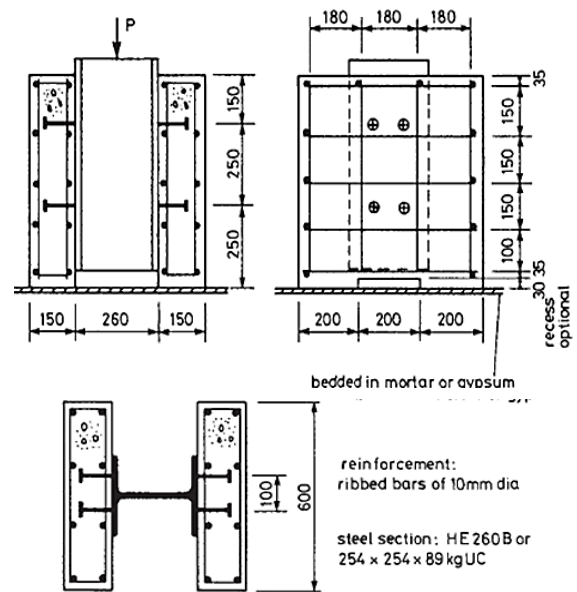


Fig. 4 Standard push-out test.

2.1. Description of test specimens

The push-out specimens' arrangements adopted in this study were a combination of the type proposed by Taylor and standard specimens described in Eurocode 4 (2004) and BS 5400 [10]. For all specimens, the depth of the reinforced concrete block was taken as 400 mm, while two values for both length and width were taken, 500 and 600 mm for length and 200 and 300 mm for width as shown in Fig. 5. Two diameters of steel bar were used to act as a shear connector. Bars of $\Phi 8$ mm and $\Phi 10$ mm are selected for stirrups because they are the most commonly used in the reinforced concrete beams. As shown in Fig. 6, specimens were arranged according to the number of connectors (stirrups) in them: 12 specimens with three connectors, 16 specimens with one connector, and 28 specimens with two connectors. Also, two sizes of steel T-section were used. These were 100 mm flange width and 100 mm total depth (Type A) and 120 mm flange width and 120 mm total depth (Type B), and 28 specimens were fabricated with each size. The length of the steel T-section is 500 mm, i.e., with 100 mm extra length over the concrete block depth to allow for a slip to take place between concrete and steel during applying load. Forty-eight specimens were cast with concrete grade C42, while the other 8 were cast with C30. Another type of specimen (denoted by II) was fabricated by changing the location of the steel T-section so that the specimen is similar to the standard push-out test, Fig. 5 (d). Eight specimens of type II were made with two and three connectors. The details of the specimens tested in experimental work done by the same researchers are listed in Table 1.

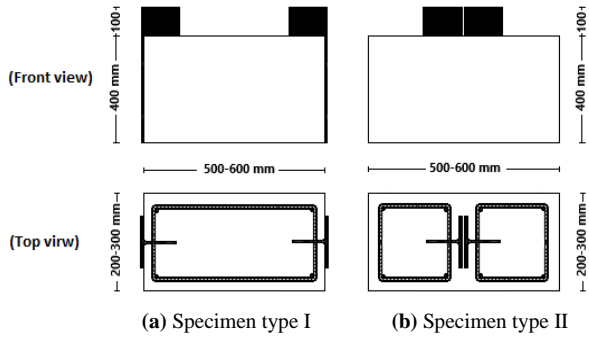


Fig. 5 Types of pushout specimens.

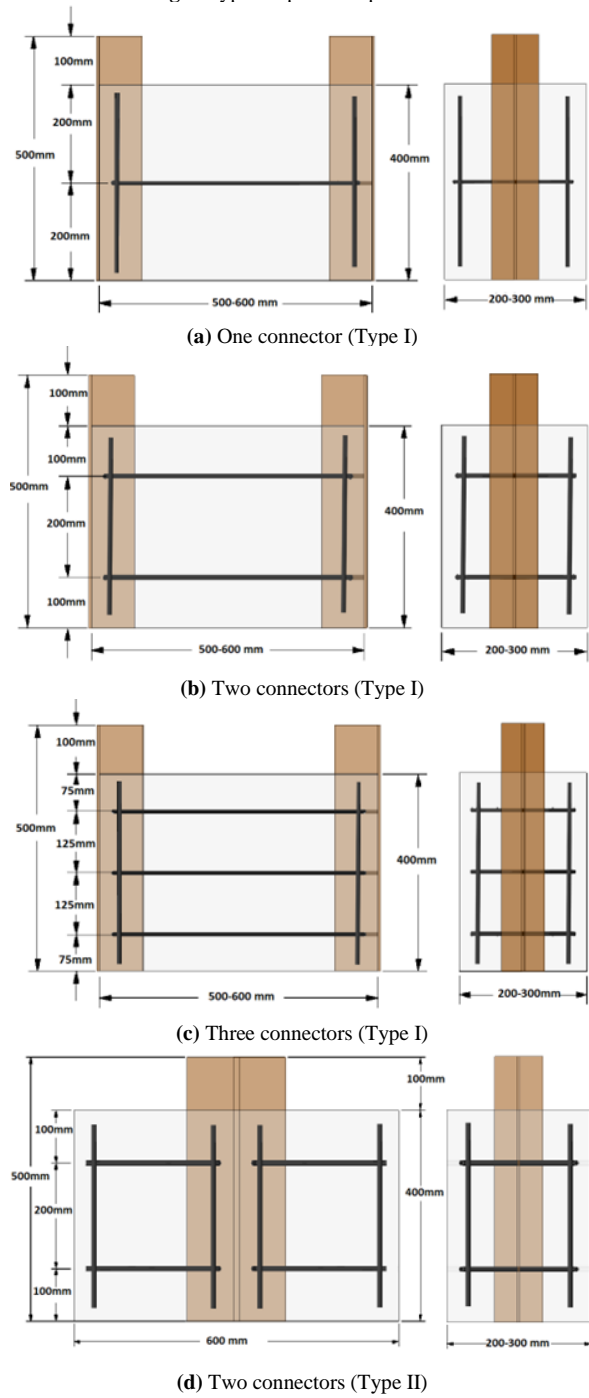


Fig. 6 Typical Pushout Specimens.

The bearing plate that was used to support specimens was made so that it could support the concrete block completely, with two slots left on both sides along the T-section web to allow the steel T-section to slip freely after loading, Fig. 7.

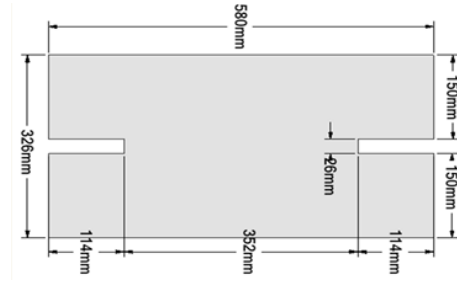


Fig. 7 Bearing plate configuration.

Table 1. Details of tested specimens.

Specimen designation	Specimen Width mm	Stirrup Dia. mm	Specimen length mm	No. of stirrups	Concrete strength MPa	Type of T-section	Type of specimen
P1	200	8	500	1	42	A	I
P2	200	8	500	2	42	A	I
P3	200	8	600	1	42	A	I
P4	200	8	600	2	42	A	I
P5	200	10	500	1	42	A	I
P6	200	10	500	2	42	A	I
P7	200	10	600	1	42	A	I
P8	200	10	600	2	42	A	I
P9	300	8	500	1	42	A	I
P10	300	8	500	2	42	A	I
P11	300	8	600	1	42	A	I
P12	300	8	600	2	42	A	I
P13	300	10	500	1	42	A	I
P14	300	10	500	2	42	A	I
P15	300	10	600	1	42	A	I
P16	300	10	600	2	42	A	I
P17	200	8	500	1	42	B	I
P18	200	8	500	2	42	B	I
P19	200	8	600	1	42	B	I
P20	200	8	600	2	42	B	I
P21	200	10	500	1	42	B	I
P22	200	10	500	2	42	B	I
P23	200	10	600	1	42	B	I
P24	200	10	600	2	42	B	I
P25	300	8	500	1	42	B	I
P26	300	8	500	2	42	B	I
P27	300	8	600	1	42	B	I
P28	300	8	600	2	42	B	I
P29	300	10	500	1	42	B	I
P30	300	10	500	2	42	B	I
P31	300	10	600	1	42	B	I
P32	300	10	600	2	42	B	I
P33	200	10	600	3	42	A	I
P34	200	8	600	3	42	A	I
P35	300	10	600	3	42	A	I
P36	300	8	600	3	42	A	I
P37	200	10	600	3	42	B	I
P38	200	8	600	3	42	B	I
P39	300	10	600	3	42	B	I
P40	300	8	600	3	42	B	I
P41	200	10	600	2	30	A	I
P42	200	8	600	2	30	A	I
P43	300	10	600	2	30	A	I
P44	300	8	600	2	30	A	I
P45	200	10	600	2	30	B	I
P46	200	8	600	2	30	B	I
P47	300	10	600	2	30	B	I
P48	300	8	600	2	30	B	I
P49	200	10	600	2	42	A	II
P50	200	10	600	3	42	A	II
P51	300	10	600	2	42	A	II
P52	300	10	600	3	42	A	II
P53	200	10	600	2	42	B	II
P54	200	10	600	3	42	B	II
P55	300	10	600	2	42	B	II
P56	300	10	600	3	42	B	II

3. Finite element analysis

A three-dimensional finite element model is created using the finite element program ANSYS 21 student version to simulate the pushout specimens for CRC system with innovative shear connectors. The GUI method was exclusively used in this numerical analysis by ANSYS 21 workbench GUI platform [11].

3.1. Material properties

ANSYS workbench has an extensive database of material properties that can be used in static analysis. The properties of steel T-section and rebar materials were added within the new data library. These properties consist of the linear elastic properties (young modulus and Poisson's ratio) which are defined under model isotropic elasticity and plasticity properties (yield stress and tangent modulus) are defined under mode bilinear isotropic hardening as illustrate in Table 2 [12].

Table 2. Properties of steel section and rebar.

Property	Steel bars		Steel T-Section
	8 mm diameter	10 mm diameter	
Young's modulus (MPa)	200,000	200,000	200,000
Poisson's ratio	0.3	0.3	0.3
Yield Stress (MPa)	410	538	350
Tangent Modulus	2000	2000	2000

The ANSYS library provides a variety of approaches to model concrete. In the current analysis, the Menetrey-Willam constitutive model [13] which is based on the Willam-Warnke yield surface [14] was used to define concrete. This method requires defining a total of 12 input parameters to facilitate the corresponding nonlinear behavior of the model. Young's modulus of elasticity E_c , Modulus of rupture R_t , and biaxial compressive strength R_b for concrete was calculated in accordance with (ACI318-19 sections 19.2.) [15]. The Poisson's ratio of concrete was taken as 0.20 (fib MC 2010 section 5.1.7.3) [16] and the dilatancy angle ψ was assumed as 30° (per common practice) [17]. Table 3 illustrates the values of these parameters and other parameters relating to linear softening which are used for the convergence of the nonlinear solution. The stress-strain curves of concrete used in this analysis resulting from the Menetrey-Willam model parameters are illustrated in Fig. 8.

3.2. Defining symmetry and contact surfaces

The experimental specimens of the push-out test were symmetrical about planes perpendicular to the length of the specimen, so only half of the specimens were modeled and a symmetry region was implemented to replicate the other half. The symmetry was defined during the analysis by one or more symmetry faces by geometry selection as well as axis normal to symmetry plane as shown in Fig. 9 (a).

The assembly model of push-out specimens has many contact surfaces between the four different components (concrete, steel section, stirrups, and bearing plate. A set of contact regions were detected and created as a pair of contact and target bodies, Fig. 9 (b). The default behavior chosen by the program for detected contact pairs is bonded type, so it was

changed manually to the appropriate contact type as presented in Table 4.

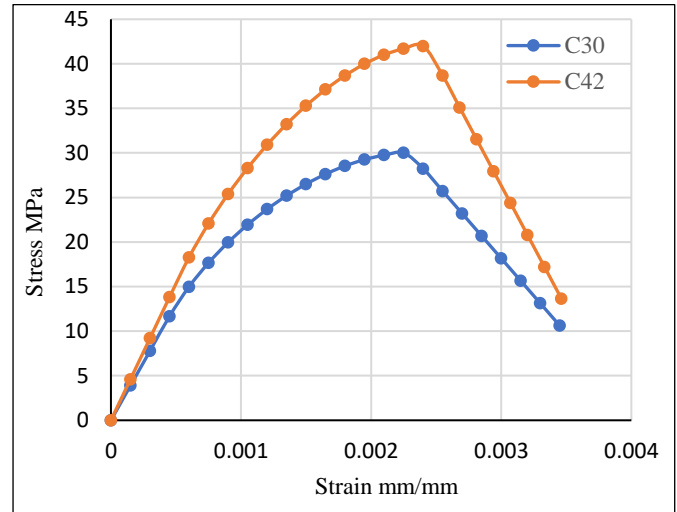
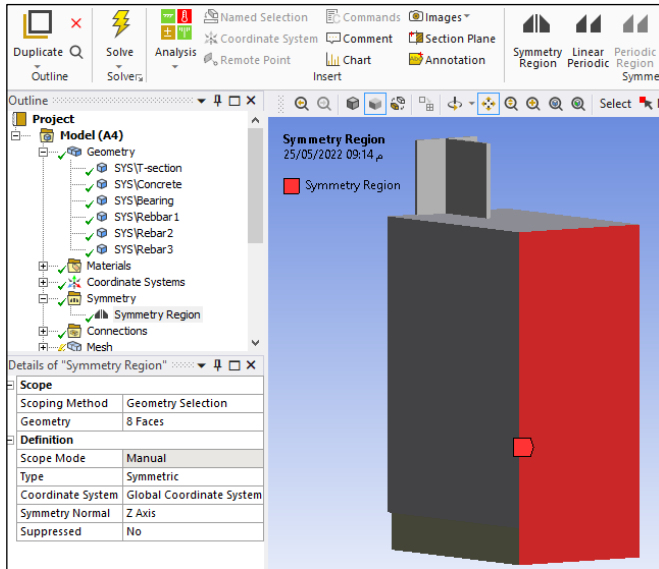


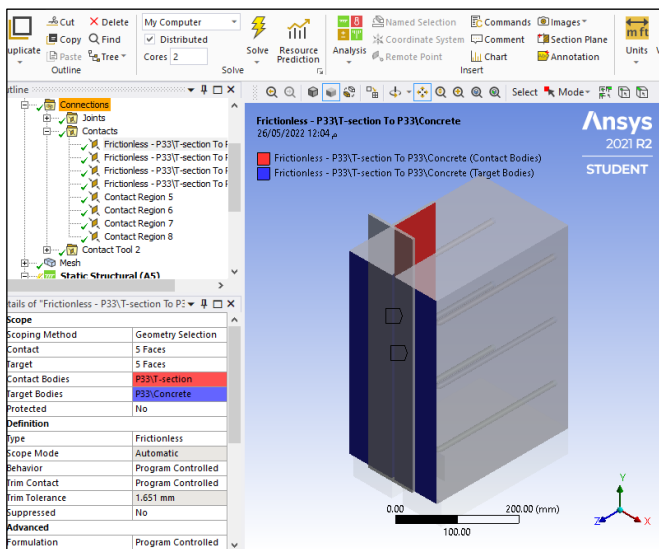
Fig. 8 Stress - strain curves for concrete.

Table 3. Menetrey-Willam model parameters for concrete material.

Property type	Unit	Parameters	Parameter Input Values	
			Concrete Grade (30)	Concrete Grade (42)
Linear isotropic	MPa	Young's modulus of elasticity	25923	30672
	-	Poisson's ratio	0.2	0.2
Yield strength	MPa	Uniaxial Compressive Strength	30	42
	MPa	Uniaxial Tensile Strength	3.41	4.04
	MPa	Biaxial Compressive Strength	35.1	48.5
The dilatancy	°	Dilatancy Angle	30°	30°
Hardening and Softening	-	Plastic strain at uniaxial compressive strength	0.00114	0.00105
	-	Ultimate effective plastic strain in compression	0.0035	0.0035
	-	Relative stress at start of nonlinear hardening	0.4	0.4
	-	Residual compressive relative stress	0.2	0.2
	-	Plastic strain limit in tension	0.0004	0.0004
	-	Residual tensile relative stress	0.01	0.01



(a) Symmetry region



(b) Contact surfaces

Fig. 9 Symmetry region and contact surfaces.

Table 4. Contact regions and corresponding types.

Contacted Bodies	Contact Type
Concrete to Stirrup (Connector)	Bonded
Steel Section to Concrete	Frictionless
Steel Section to Stirrups (Connector)	Frictionless
Concrete to bearing plate	Bonded

3.3. FE meshing and elements types

The push-out models in this analysis have been meshed with automatic mesh generation. Three-dimensional solid elements have been utilized in order to achieve accurate results. The element type for model bodies was automatically selected by the program based on some predefined features on the mesh control window including material properties, element order, physics preference...etc. Fig. 10 illustrates automatic meshing executed for push-out model.

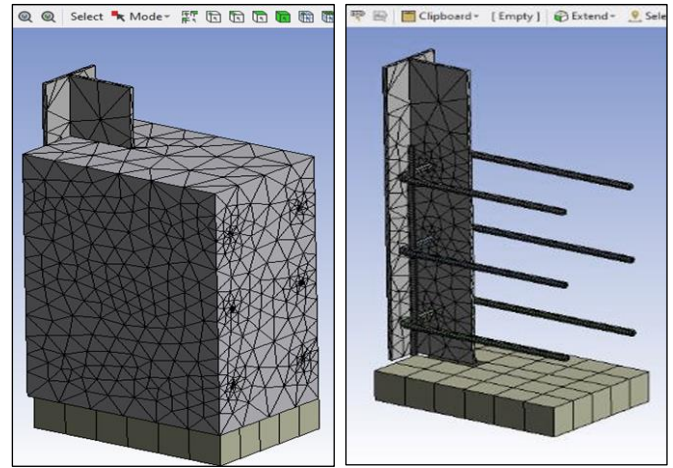


Fig. 10 The push-out model mesh.

Based on the input data, program has specified a three-dimensional eight-node element SOLID185 for the concrete, shear connector, and the bearing plate, while three-dimensional four-node Tetrahedral Structural Solid element SOLID285 has been specified for the steel T-section. 3-D 8-Node Surface-to-Surface element CONTA174 and 3-D Target Segment element TARGE170 has been specified for model contact pairs.

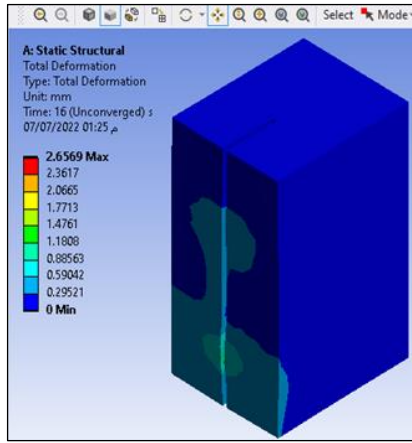
4. FE models results and comparison

The theoretical results and the comparison with the experimental results are presented and discussed in this section. The FE analysis has been performed in this study to predict of the connector strength, load versus slip response, and failure modes of the innovative shear connectors in the new CRC system. A total of fifty-six FE models have been analyzed and discussed within this section. The following comparisons are made: specimens failure modes, connector strength and slip at maximum load, and the behavior of the load-slip curves.

4.1. Failure modes

The finite elements analysis using the ANSYS vs.21.2 program gives the intensity and shape of deformations that occur in all model parts and at any load step. For example, Fig. 11 shows the contour distribution and deformed shape of all parts of the model (P2) at the failure load level obtained using ANSYS program.

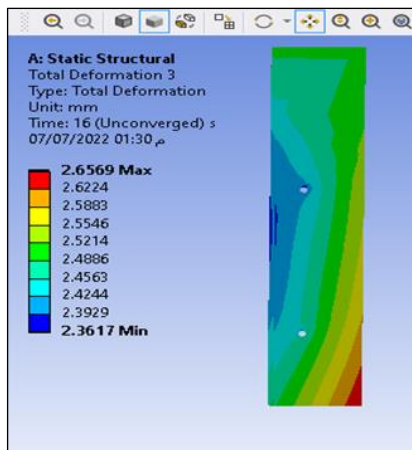
Theoretical analysis showed a good ability to predict the form and intensity of deformations in the model when compared with the deformations that occurred in the corresponding experimental specimen. A great similarity has been observed between them. Figure 12 shows a comparison between an experimental specimen (P12) and the corresponding FE model at the failure stage.



(a) Concrete block.



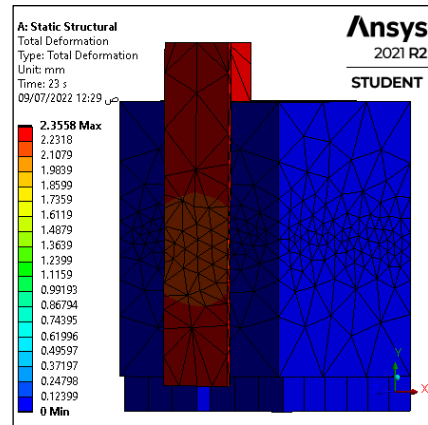
(b) Shear connectors.



(c) Steel T-section.

Fig. 11 The deformation of all parts of FE model.

Failure Modes 1: This failure results from the fracture of the shear connector occurred in the specimens made with a connector of small diameter, especially those that contained a single connector and had a relatively large width. The crushing of concrete was limited to local concrete underneath connectors and do not spread extensively on both sides of the steel section. Figure 13 illustrates a comparison between the failure of the FE model and the corresponding experimental specimen (P27).



(a) FE Model.

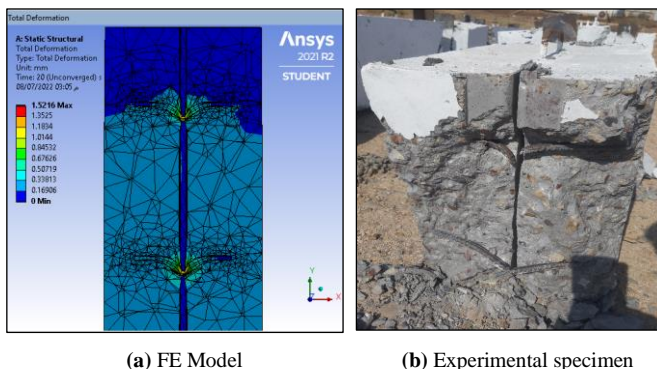


(b) Experimental specimen.

Fig. 13 Experimental and FE failure comparison of specimen P27.

Failure Modes 2: The main feature of this mode of failure was shearing of the concrete in a conical shape around the shear connector. It results from the cracking and crushing of concrete in front of the shear connector due to a very high concentration of stresses within a smaller area. When the connector diameter is large and has high strength, greater crushing occurs in the surrounding concrete. The cracks and crushing continue to spread outward through the thickness of the concrete with the help of the separation force which causes the concrete to shearing in a conical shape around the shear connector. Figure 14 illustrates a comparison between the FE model and the corresponding experimental specimen (P32).

Failure Modes 3: The main feature of this mode of failure was the shearing of the concrete on both sides of the steel section. It was dominant in the Push-out specimens manufactured with three shear connectors, especially those that had a small width. The failure mechanism occurs as a result of the spread of cracks that develop in the concrete underneath the connector. These cracks forming a longitudinal crack that results in the separation of concrete on both sides. This type of failure was dominant in most of the specimens which were manufactured



(a) FE Model

(b) Experimental specimen

Fig. 12 Comparison between experimental and FE deformations.

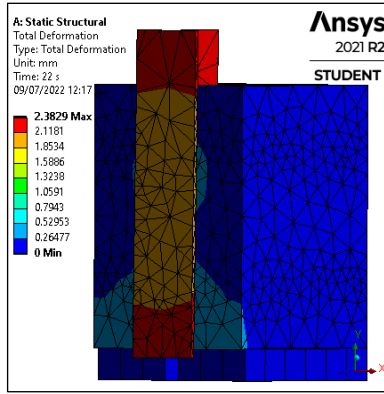
with three shear connectors where the spacing between the connectors was 125 mm. The comparison between the FE model and the corresponding experimental specimen (P37) is illustrated in Fig. 15.

4.2. Connector shear strength

The results obtained from finite element analysis were compared with those of experimental push-out tests as shown in Table 5. The experimental and finite element connector strength was denoted by P_{Test} and P_{FE} respectively.

Table 5. Comparison between experimental and FEA results of the connector strength.

Specimen	P_{Test} (N)	P_{FE} (N)	$\frac{P_{Test}}{P_{FE}}$	Specimen	P_{Test} (N)	P_{FE} (N)	$\frac{P_{Test}}{P_{FE}}$
P1	55000	58500	0.94	P29	75500	76500	0.99
P2	48000	54000	0.89	P30	77000	86000	0.90
P3	60000	54500	1.10	P31	95500	90500	1.06
P4	51000	48000	1.06	P32	78000	87000	0.90
P5	68000	67500	1.01	P33	63250	72000	0.88
P6	62000	72000	0.86	P34	46500	51000	0.91
P7	69000	68000	1.01	P35	66000	74500	0.89
P8	68500	68000	1.01	P36	48000	55500	0.86
P9	63500	57000	1.11	P37	58500	65500	0.89
P10	59500	56500	1.05	P38	43500	50000	0.87
P11	66000	62000	1.06	P39	62000	73250	0.85
P12	61000	59500	1.03	P40	47500	53500	0.89
P13	92500	89000	1.04	P41	55000	61000	0.90
P14	83000	86000	0.97	P42	49000	50000	0.98
P15	88000	84500	1.04	P43	67000	73000	0.92
P16	76000	85000	0.89	P44	48500	51500	0.94
P17	54000	57400	0.94	P45	57000	63000	0.90
P18	48500	50000	0.97	P46	46500	50800	0.92
P19	56000	56000	1.00	P47	64500	70000	0.92
P20	54000	59500	0.91	P48	46500	51400	0.90
P21	65000	69500	0.94	P49	67500	73000	0.92
P22	63500	73500	0.86	P50	61500	69000	0.89
P23	64000	68000	0.94	P51	74000	83500	0.89
P24	65500	73500	0.89	P52	61000	73500	0.83
P25	64000	60300	1.06	P53	63000	71000	0.89
P26	55500	60500	0.92	P54	54500	62500	0.87
P27	58500	63000	0.93	P55	71000	81500	0.87
P28	52000	58500	0.89	P56	57000	63000	0.90

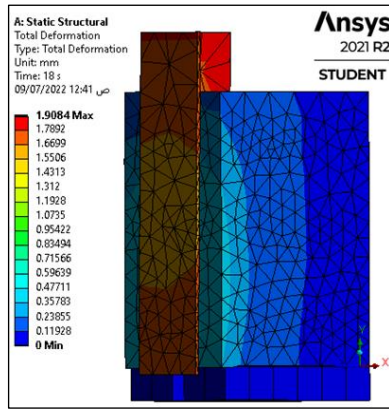


(a) FE Model.



(b) Experimental specimen.

Fig. 14 Experimental and FE failure comparison of specimen P32.



(a) FE Model.

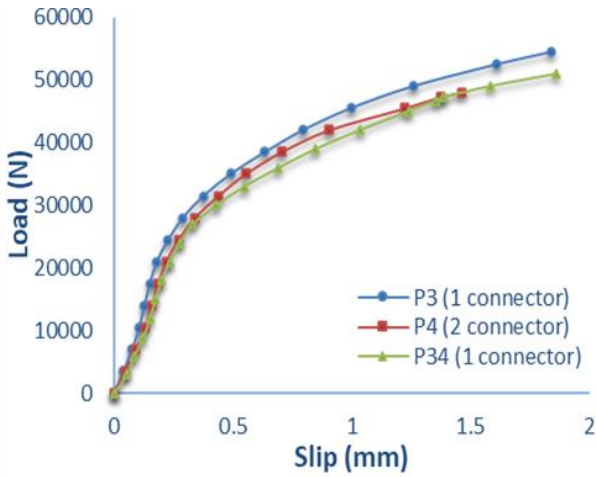


(b) Experimental specimen.

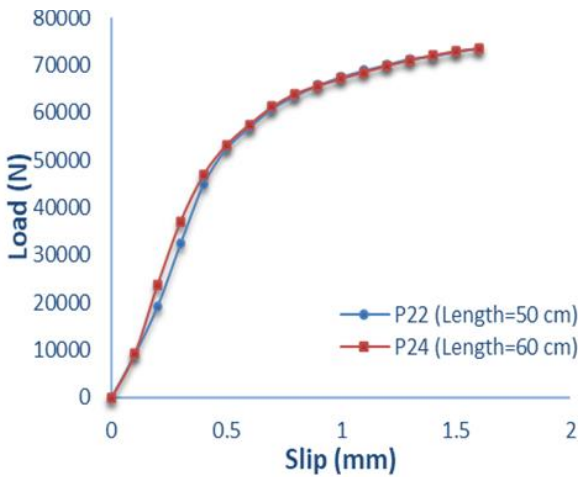
Fig. 15 Experimental and FE failure comparison of specimen P37.

The results obtained from the finite element analysis using the ANSYS program showed close agreement with the experimental results obtained from push-out tests in terms of shear connector strength. The maximum difference in connector strength which was observed between the numerical and experimental results was 15 %. The mean of the experimental to the numerical values of connector strength is 0.94. The difference in connector strength was greater for the specimens that had a large number of shear connectors. The group of specimens P33 to P40 which were made with three connectors showed larger differences in connector strength, ranging from (9 % - 15 %).

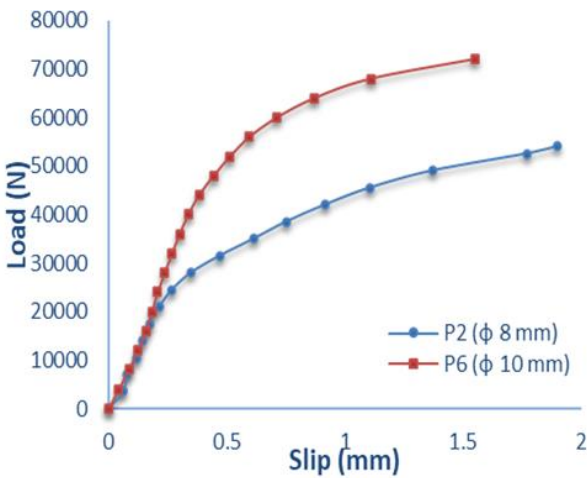
The good prediction of finite element analysis using ANSYS program was not only limited to connector strength and slip, but was also good in predicting the effect of studied parameters on connector strength. It was noted that the parameters that had a significant effect were the diameter of the connector, concrete strength, and model width, for which their increase directly affects the resistance of the connector. The other parameters showed slight effects. Figure 16 illustrate the parameter effects according to the FEA results.



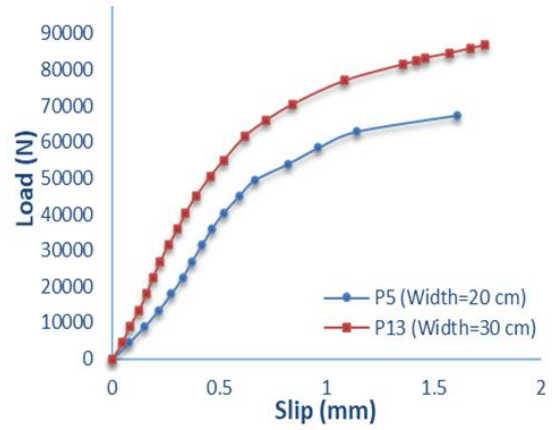
(a) No. of connectors per specimen.



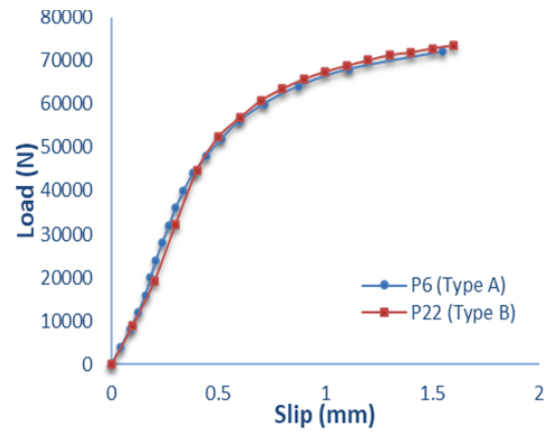
(b) Specimen length.



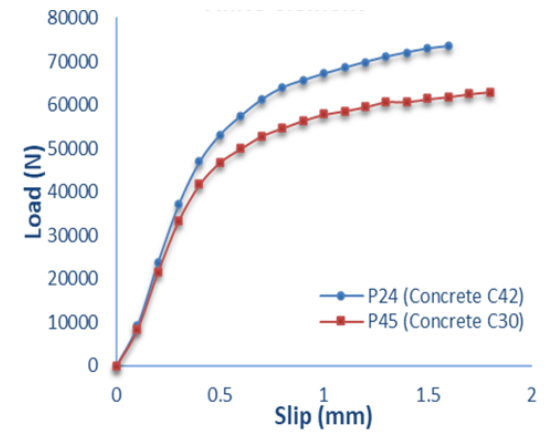
(c) Connector diameter.



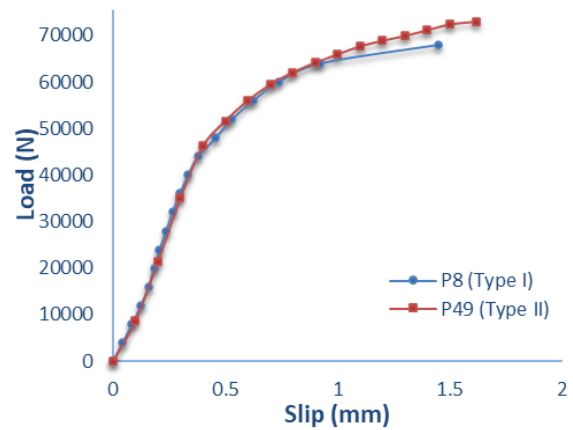
(d) Specimen width.



(e) Size of T-section.



(f) Concrete strength.



(g) Specimen shape.

Fig. 16 Effect of studied parameters on connector strength.

4.3. Load-slip response

The load-slip curves obtained from the finite element analysis showed good agreement in general behavior with the experimental results. The load-slip curves determined by FE analysis were stiffer than the experimental curves, Fig. 17. The difference in stiffness was related to boundary conditions and the constraint for the models in finite element analysis and the manufacture of holes in the steel section through which the connector passes. The diameter of these holes was slightly larger than the diameter of the connector in experimentally tested specimens.

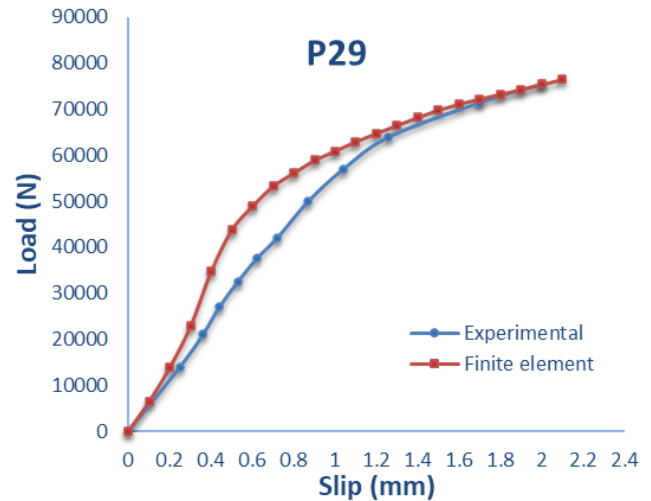
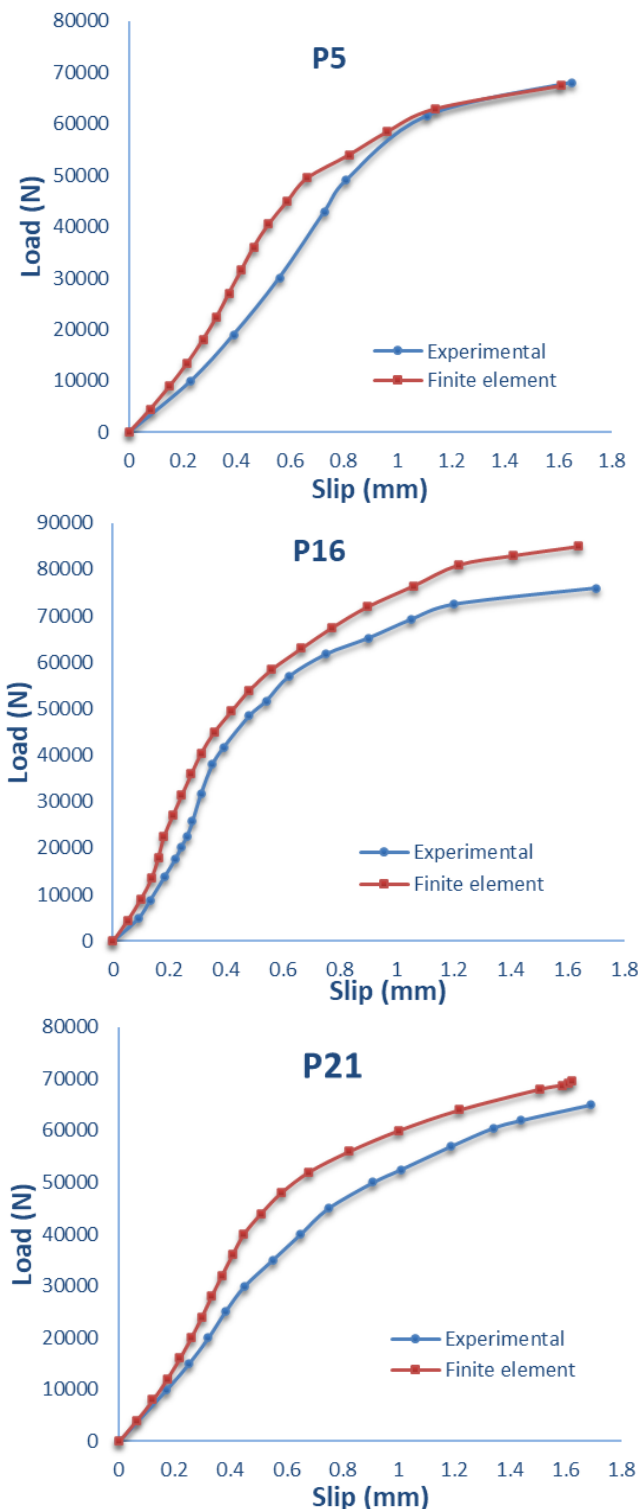


Fig. 17 Comparison between experimental and FE analysis results.

5. Conclusions

The following main conclusions are drawn based on the results from the analysis of finite elements:

1. The suggested model shows a good ability to predict the form and intensity of deformations when compared with the deformations that occurred in the corresponding experimental specimens.
2. The failure modes of models predicted by FE analysis show good similarity to those occurring in the corresponding specimens in the experimental work.
3. The load-slip curves obtained from the finite element analysis show close response to that of experiment tests. The load-slip curves evaluated by FE analysis are stiffer in the linear stage than the experimental curves.
4. The results obtained from the finite element analysis using the ANSYS program show close agreement with the experimental results obtained from Push-out tests in terms of shear connector strength. The maximum difference in connector strength which is observed between the numerical and experimental results is 15 %.
5. The finite element analysis using ANSYS shows good prediction for the effect of studied parameters on connector strength. The parameters having a significant effect are the diameter of the connector, concrete strength, and model width. The other parameters show slight effects.

References

- [1] R. P. Johnson, Composite Structures of Steel and Concrete: beams, slabs, columns and frames for buildings, Third Edition, Wiley-Blackwell Scientific Publications, Oxford, UK, 2004.
- [2] R. Taylor, Composite reinforced concrete, Thomas Telford Limited, London, 1979.
- [3] R. Taylor, and P. Cunningham, "Tests on the Transverse Connector for the Composite Reinforced Concrete", Proceedings of the Institution of Civil Engineers, Vol. 63, Issue 4, pp. 913-920, 1977. <https://doi.org/10.1680/icep.1977.3086>
- [4] D. A. U. Witwit, and N. A. Jasim, "Torsional Capacity of Composite Reinforced Concrete Beams with Stirrup Connectors", Anbar Journal of Engineering Sciences, Vol. 9, Issue 2, pp. 177-192, 2021. <https://doi.org/10.37649/aengs.2021.171186>

- [5] D. A. U. Witwit, and N. A. Jasim, "Assessment of the flexural capacity of composite reinforced concrete beams using experimental tests and finite element analysis", *Journal of Physics: Conference Series*, Vol. 1895, pp. 1-15, 2021. <https://doi.org/10.1088/1742-6596/1895/1/012066>
- [6] D. A. U. Witwit, and N. A. Jasim, "Behaviour of New Curved in Plan Composite Reinforced Concrete Beams", *Basrah Journal for Engineering Sciences*, Vol. 22, No. 2, pp. 80-89, 2022. <https://doi.org/10.33971/bjes.22.2.12>
- [7] H. R. Lazim, and N. A. Jasim, "Pushout Test on Stirrup Shear Connector in New Steel Concrete Composite System", Accepted for publication in the conference proceedings of ICES2022, AIP Conference Proceedings publisher, 2023.
- [8] Q. Q. Liang, *Analysis and design of steel and composite structures*, Boca Raton and London: CRC Press, Taylor and Francis Group, ISBN-13: 978-0-415-53220-4, 2015.
- [9] European Committee for Standardization. EUROCODE 4, Design of composite steel and concrete structures-Part 1.1: General rules and rules for buildings. Pr EN 1994-1-1, 2004.
- [10] BS5400, B. S. Steel, concrete and composite bridges, Part 5, Code of practice for design of composite bridges. British Standards Institution, London, 1979.
- [11] Workbench, A. N. S. Y. S. Release 21.2 Workbench User's Guide. Ansys Inc., Canonsburg, PA, USA, 2021.
- [12] ANSYS Mechanical User's Guide, Release 2021 R2, ANSYS Inc., Canonsburg, PA, USA, 2021.
- [13] P. Menetrey, and K. J. Willam, "Triaxial failure criterion for concrete and its generalization", *Structural Journal*, Vol. 92, Issue 3, pp. 311-318, 1995. <https://doi.org/10.14359/1132>
- [14] K. W. E. Warnke, and E. P. Warnke, "Constitutive model for triaxial behaviour of concrete", *Proc. Concrete Structure Subjected to Triaxial Stresses*, Int. Ass. for Bridge and Structural Engineering, Zurich, 1-30, 1975.
- [15] J. P. Moehle, and G. M. Zeisler, Building code requirements for structural concrete (ACI 318-19), commentary on building code requirements for structural concrete (ACI 318R-19), American Concrete Institute ACI standard, 2019.
- [16] FIB (Fédération Internationale du Béton), First complete draft-Volume 1, Model code 2010.
- [17] J. Lubliner, J. Oliver, S. Oller, and E. Oñate, "A plastic-damage model for concrete", *International Journal of Solids and Structures*, Vol. 25, Issue 3, pp. 299-326, 1989. [https://doi.org/10.1016/0020-7683\(89\)90050-4](https://doi.org/10.1016/0020-7683(89)90050-4)